JGR Space Physics

RESEARCH ARTICLE
10.1029/2019JA026625

Key Points:
- We derive an analytic formulation of the electron cloud surface charge associated with the solar wind plasma wake at a lunar crater
- New boundary conditions for plasma expansion provide physical insight into the steady-state condition near the lunar surface
- The solution describes a unique nonneutral electrical environment in shadowed regions of the Moon

Correspondence to:
D. J. Rhodes,
dovjr6@gmail.com

Citation:
Rhodes D. J., & Farrell, W. M. (2019). Steady-state solution of a solar wind-generated electron cloud in a lunar crater. *Journal of Geophysical Research: Space Physics*, *124*, 4983–4993. https://doi.org/10.1029/2019JA026625

Received 19 FEB 2019
Accepted 16 JUN 2019
Accepted article online 4 JUL 2019
Published online 22 JUL 2019

©2019. The Authors.
This is an open access article under the terms of the Creative Commons Attribution License, which permits use, distribution and reproduction in any medium, provided the original work is properly cited.
This article has been contributed to by US Government employees and their work is in the public domain in the USA.

Steady-State Solution of a Solar Wind-Generated Electron Cloud in a Lunar Crater

Dov J. Rhodes[1] **and W. M. Farrell**[1]

[1]NASA Goddard Space Flight Center, Greenbelt, MD, USA

Abstract We formulate an analytic description of a steady-state electron cloud and affiliated surface charge, formed in the plasma wake generated as the solar wind flows horizontally over a lunar crater. The solution is complementary to the well-known self-similar plasma expansion formulation, which breaks down at the plasma wake front and thus fails to capture a substantial region of the crater interior. The present model establishes a theoretical basis for existing simulation results, which suggest that the cavity formed below the wake front is populated mainly by electrons, resulting in a substantial negative surface charge. The electrostatic potential throughout this subwake region is determined by solving Poisson's equation for a Maxwellian electron cloud, bounded above by the self-similar plasma expansion front and below by the electrostatically charged surface.

1. Introduction

As the solar wind flows over the varying topography of the lunar surface, it is predicted to form nonneutral plasma wakes which result in the buildup of local space charge, surface charge, and electrostatic fields (Farrell et al., 2007, 2008a, 2010; Zimmerman et al., 2011). Experimental evidence of this effect was first observed by the Lunar Prospector (Halekas et al., 2002). Similar plasma wakes arise in comparable airless environments such as asteroids (Poppe et al., 2015; Zimmerman et al., 2014), the moons of Mars (Farrell et al., 2017), and around spacecrafts (Ergun et al., 2010). The present paper provides an analytic description of the steady-state plasma wake structure in a lunar crater, immediately downstream from a topographical obstruction.

The interest in this orographic plasma wake effect is motivated by a number of secondary processes, including dust transport (Poppe et al., 2012; Stubbs et al., 2006), surface sputtering (Killen et al., 2012), and nonuniform distribution of volatile materials (Farrell et al., 2010). In addition, the resulting environment poses a possible challenge to human explorers and their equipment, owing to the inability to dissipate electrostatic charge that accumulates by triboelectric surface interaction (Farrell et al., 2008b; Jackson et al., 2011, 2015). Since the surface of the Moon is electrically insulating, the main source of electrical grounding is the ambient plasma. Unlike on the dayside of the Moon where the accumulated charge on astronauts and rovers is largely dispersed by photoelectric and charge exchange interactions, the plasma-depleted nightside and permanently shadowed regions of the Moon lack a reliable source of electrical grounding.

The low dissipation regions are predicted to persist in permanently shadowed regions of the Moon (or other airless bodies). Of particular relevance to human exploration is the lunar polar region, where craters containing water ice may permanently reside in shadow and interact only with a horizontally streaming solar wind. The Moon's nightside is expected to temporarily develop such conditions as well, since a steady-state plasma wake is attained along the lunar terminator much faster than the rotation timescale of the Moon. In these regions, a residual surface charge distribution is likely to persist until the return to daylight. While no in situ measurements have been made on the shadowed lunar surface, analogous plasma wakes have been observed on a macroscopic scale around the Moon (Ogilvie et al., 1996), as well as on microscopic scales around spacecrafts (Tribble et al., 1989).

The physics of the solar wind plasma wake can be understood through the system's characteristic timescales. The approximate bulk solar wind speed at the Moon is $V_{sw} = 4{\times}10^5$ m/s. In comparison the electron thermal and ion acoustic speeds at $T_e = 11$ eV are, respectively, $V_{Te} = 1.4 \times 10^6$ m/s and $C_i = 3.2 \times 10^4$ m/s. Given that $C_i \ll V_{sw} \ll V_{Te}$, thermal electron motion can fill a 1-km deep crater on a timescale of milliseconds, $\sim$O(10^{-3} s), while the ion thermal timescale for reaching the surface, $\sim$O(10^{-1} s), allows ample time for

the ions to traverse a large horizontal distance, ∼O(10 km). The result is a cavity populated predominantly by a nonneutral cloud of electrons. Although electron-ion charge separation forms an ambipolar potential, which accelerates the expansion of ions into the crater, initial analytic calculations by Farrell et al. (2007) and simulations by Zimmerman et al. (2011) predict a substantial electron cloud region, directly downstream of an obstructing crater or mountain.

This paper is the first to formulate a theoretical model for the surface charge and near-surface electron cloud environment in the wake of a lunar crater. Previous studies such as Farrell et al. (2010) and references therein rely on a 1-D self-similar plasma expansion model (Gurevich et al., 1966; Mora & Pellat, 1979), projected onto a 2-D wake structure based on a uniform solar wind flow velocity. It is known, however, that the quasi-neutral self-similar model breaks down at the expansion wake front (Mora, 2003; Samir et al., 1983). In the present work, we complement the existing studies by explicitly addressing the electron cloud region beyond the expansion front, that is, beyond the validity of the self-similar model. In previous work (Farrell et al., 2007, 2010), regions where electron clouds could form were identified, but a closed solution for the surface potential could not be obtained in these regions. They instead invoked a new physical process of negatively charged dust lofting to obtain a countercurrent required for a closed solution. As mentioned above, Zimmerman et al. (2011) observed an electron cloud in a 2-D kinetic code and obtained an estimate of the surface charge (see their Figure 2). As described therein, the estimate of surface charge state was not fully closed, since it was limited to the most energetic electrons modeled in the simulation. Up until this work, an analytic solution for the electron cloud and related surface charge steady state had yet to be derived, and this is the primary objective herein. Once analytically understood, this solution can be dovetailed back into larger codes such as that of Farrell et al. (2010).

Inspired by a nonneutral expansion model by Crow et al. (1975), which combines a numerical solution of the expanding plasma with an analytic solution of the electron cloud, we generate a purely analytic approximation by matching components of the self-similar and nonneutral solutions along a sharp expansion front. The sharp-boundary matching conditions enforce potential and electron density continuity, while permitting the usual self-similar discontinuity of expansion front ion density and electric field. The electric field jumps correspond to thin layers of positive surface charge, which balance the negatively charged electron cloud and thus maintain overall charge neutrality. The resulting analytic model allows us to compute the electron cloud space charge distribution within a crater with finite boundary conditions, consistent with the expanding ion wake above, as well as the resulting surface charge at the crater floor. This analytic approach affords us the ability to rapidly compute the surface potential and near-surface environment (versus running computationally heavy particle-in-cell plasma codes), as well as to easily adapt the boundary conditions and incorporate additional physics in future variations of the model.

A laboratory example of an electrostatically confined pure electron plasma, called an electron sheath, is formed at the plasma interface of a positively charged surface (Scheiner et al., 2015). As described herein, two key features differentiate the presently studied electron cloud from an electron sheath: (i) The electron cloud can be much larger than the typical Debye length scale for plasma charge separation, and (ii) the electron cloud produces a negative floating potential at the surface. These features make the electron cloud qualitatively distinct from the previously studied laboratory phenomenon of the electron sheath.

The simple fluid model presented here builds on the aforementioned literature, while opening an avenue for new studies focused specifically on the electron cloud environment in a lunar crater. One caveat of this fluid model is that it fails to accurately resolve the full extent of the surface charge, owing to the absence of kinetic effects. Although the equilibrium surface potential repels thermal electrons, supra-thermal electrons in the tail of the velocity distribution will continue to penetrate the electric field at the surface, charging the surface more negatively than predicted by the fluid force balance. Similar nonlinear surface effects are found in Gurevich and Pitaevsky (1975). A second caveat to be addressed in further extensions of this work is the assumption of a Maxwellian solar wind plasma, which might be more accurately portrayed by a κ-distribution (Halekas et al., 2005). In addition, 3-D topographical effects may change the local surface charge but are not expected to qualitatively affect the overall electron cloud structure within a large crater, especially when the crater wall is relatively steep. Additional physical processes, such as secondary electrons and dust lofting, may substantially alter the electron cloud (Zimmerman et al., 2011). These additions are left for future work.

The paper is organized as follows. Section 2 reviews the application of a self-similar solution to the wake structure within the quasi-neutral plasma. Section 3 describes the model of a 1-D electron cloud fluid equilibrium and matches it in sequence to the boundary of the 2-D wake structure provided by the known self-similar solution. Section 4 presents calculations of an idealized lunar crater with typical solar wind conditions as 1 AU, and section 5 contains a summary of the main points.

2. Adaptation of 1-D Self-Similar Formulation to a 2-D Wake

Consider a diffuse quasi-neutral plasma flowing horizontally over an airless crater. This situation occurs at the Moon for craters located at the terminator, including the polar regions. Within the crater, the effects of neutral gas, radiation or anomalous magnetic fields are taken to be negligible. The interplanetary magnetic field is also neglected, since the resulting electron gyroradius is much larger than the typical length scales of this system (Zimmerman et al., 2011). Thus, the predominant effects are governed by the electrostatics of plasma expansion into a vacuum. As in the work of Farrell et al. (2010), the quasi-neutral plasma wake structure can be approximated by a self-similar plasma expansion model (Gurevich et al., 1966; Mora & Pellat, 1979). We briefly review this quasi-neutral wake formulation, along with its finite bounds of validity (Mora, 2003; Samir et al., 1983) and adaptation to the 2-D wake structure (Farrell et al., 2010).

Assuming cold ions and a Maxwellian electron distribution, the combination of the ions' equation of motion and continuity equation produces a self-similar structure, in terms of a dimensionless parameter $\xi \equiv \zeta/C_i t$, where ζ is the expansion direction and C_i is the ion thermal speed. The resulting solution is

$$v/C_i = \xi + 1, \qquad n/n_{e0} = e^{-(\xi+1)}, \qquad \frac{e\phi}{kT_e} = -(\xi + 1). \tag{1}$$

The quasi-neutral expansion velocity $v = \mathrm{d}\zeta/\mathrm{d}t$ is defined by the direction of the expansion variable ζ. In the present case we will set $\zeta = -z$, since the plasma expands downward into the crater. The plasma density n, equal for electrons and ions in this region, is defined relative to the undisturbed plasma electron density n_{e0}. The assumption that the electron temperature remains constant is justified by the parameter space of the present application. While the work of Mora and Pellat (1979) showed that a noticeable departure from an isothermal Maxwellian electron distribution may appear for $\xi \gg 1$, the present paper considers a domain where $\xi < 4$, where constant temperature remains a reasonable approximation.

Requiring that the expansion length scale exceed the local Debye length (Mora, 2003; Samir et al., 1983), this solution is limited to the quasi-neutral wake region where

$$-1 < \xi < -1 + 2\ln\left(\omega_i t\right), \qquad \omega_i t \geq 1. \tag{2}$$

Here $\omega_i = C_i/\lambda_{D0}$ is the ion plasma frequency, which characterizes the ion dynamics, defined by the Debye length $\lambda_{D0} = (\epsilon_0 kT_e/n_{e0}e^2)^{1/2}$ of the undisturbed plasma.

Following Farrell et al. (2010), the 2-D structure comes about by relating the time variable with the horizontal dimension, $t = x/V_{\mathrm{sw}}$, assuming a fixed horizontal solar wind speed V_{sw}. Since the plasma is expanding into the crater in the direction $-z$, the self-similar parameter can be written as

$$\xi = \frac{-Mz}{x}, \qquad M = V_{\mathrm{sw}}/C_i, \tag{3}$$

in terms of the ion Mach number M. Normalizing the spatial variable $z = \lambda_{D0}\tilde{z}$ and $x = \lambda_{D0}\tilde{x}$, the quasi-neutral wake bounds are expressed as

$$\left[1 - 2\ln\left(\frac{\tilde{x}}{M}\right)\right]\frac{\tilde{x}}{M} < \tilde{z} < \frac{\tilde{x}}{M}, \qquad \frac{\tilde{x}}{M} \geq 1. \tag{4}$$

Figure 1 illustrates how the wake is bounded above by a rarefaction wave expanding linearly into the undisturbed solar wind and below by an expansion front that is accelerated toward the surface by the negative space charge of the electron cloud. Combining the wake bounds in equation (4) with the self-similar solution in equation (2), we obtain the plasma parameters at the wake front and rear. The wake front parameters define the upper boundary condition for the electron cloud region.

There is a subtlety in adapting the 1-D time-dependent self-similar solution into a 2-D steady-state wake structure. As fresh solar wind streams constantly into the system, a fresh supply of electrons circulates into

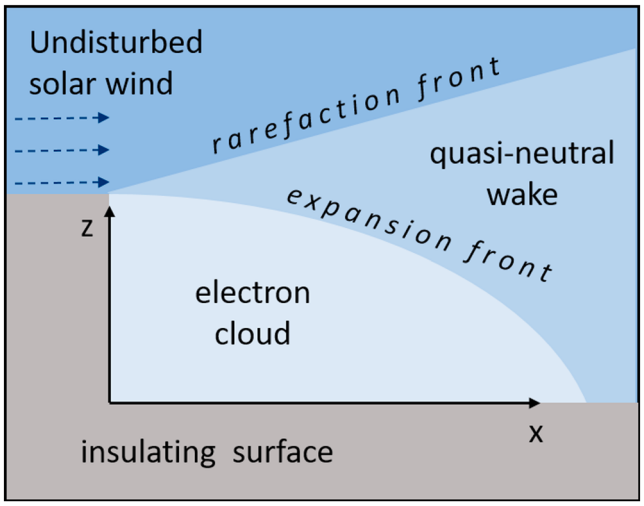

Figure 1. As the solar wind flows horizontally over a lunar crater, a quasi-neutral plasma wake is formed, bounded above by a rarefaction front at the undisturbed plasma and below by the expansion front at the electron cloud.

the electron cloud region. Similarly, electrons in the cloud are attracted back into the bulk plasma by the ambipolar potential. The resulting particle balance yields a steady-state electron cloud, which emulates the initial condition described by (Crow et al., 1975). As shown in simulations by Zimmerman et al. (2011; see their Figure 2), this circulation of incoming and outgoing electrons is most pronounced along the expansion front region that lies just beyond the obstacle. A fresh stream of undisturbed solar wind plasma provides a sharp discontinuity with the electron cloud. Here the width of the ion front boundary layer is truly negligible and our sharp-boundary approximation is accurate.

As a result, the most substantial nonneutral region of the crater is found close into the crater wall, on the left-hand side in Figure 1. This result is demonstrated in Figure 4 and is consistent with the findings in Figure 2 of Zimmerman et al. (2011). While the sharp-boundary approximation may become less accurate farther downstream as the ion front boundary layer expands (Medvedev, 2011), we nevertheless include this region in our results in order to illustrate the full wake structure.

Overall charge neutrality in the present model is maintained by a δ-function ion front layer, associated with the electric field jump along the expansion front. This positive charge layer can be thought of as an image charge induced along the interface of the electron cloud and the conducting plasma fluid. It is a self-consistent feature that naturally forms out of the presence of a negative charge below a conductor.

The following section describes the analytic extension of the self-similar wake into the electron cloud.

3. Extension Into the Electron Cloud

Given the relatively high ion Mach number, $1 \ll M$ in equation (3), there is a region behind a crater wall that is largely inaccessible to ions. This gap beyond the quasi-neutral expansion front is filled by an electron cloud—depicted in Figure 1—as shown in simulations by Zimmerman et al. (2011). While diffuse, this electron cloud is predicted to play a significant role in the electrical grounding of future exploration equipment (Zimmerman et al., 2012).

Our particular focus is in the *steady-state* condition of the crater surface-charge and near-surface environment created by the plasma wake electron cloud, assuming a constant flux of solar wind. In this case the upper bound of the electron cloud, given by the plasma expansion front $z_f(x)$, is taken to have a time stationary electron density n_{ef} and corresponding potential ϕ_f. At each horizontal cross-section x, the upper boundary potential ϕ_f is determined by the expansion front of the self-similar solution described in the previous section. The lunar surface $z = S$, on the other hand, is an electrical insulator (conductivity 10^{-14}–10^{-9} S/m; Carrier et al., 1991), which develops a surface charge σ_S dependent on the solar wind properties and crater geometry. In this simple fluid formulation, the surface charge is uniquely determined by maintaining pressure balance throughout the electron cloud column. Thus, a steady-state expression is obtained by solving Poisson's equation subject to the boundary conditions

$$\phi(z = z_f) = \phi_f, \tag{5}$$

$$\frac{\mathrm{d}\phi}{\mathrm{d}z}(z = S) = -\frac{\sigma_S}{2\epsilon_0}. \tag{6}$$

The other boundary parameters $\mathrm{d}\phi/\mathrm{d}z(z = z_f)$ and $\phi(z = S)$ are uniquely determined by the solution. These boundary conditions exhibit an important distinction from those of Crow et al. (1975), namely that the expansion regime is *finite* and bounded—both above and below—by a nonzero surface charge.

We assume that the electron cloud is reasonably approximated by a Maxwellian distribution (Crow et al., 1975; Mora, 2003). This approximation is physically justified by Halekas et al. (2005), which discusses how a

potential-filtered Maxwellian distribution remains Maxwellian. Since a Maxwellian distribution reasonably describes the self-similar region, as discussed in the previous section, it follows that it is maintained in the nonneutral region as well.

Continuing the self-similar solution into a Maxwellian electron cloud, the potential must satisfy the 1-D Poisson equation with no ion component:

$$\epsilon_0 \frac{\mathrm{d}^2\phi}{\mathrm{d}z^2} = en_{ef} \exp(e\phi/kT_e). \tag{7}$$

Here z is the vertical dimension, with the upper bound electron density n_{ef} is defined at the quasi-neutral plasma expansion front $z = z_f$, that is, the expansion front in Figure 1.

While a family of solutions is available for different values of σ_S, we are interested in a unique steady-state solution. The electrons are assumed to charge up the insulating surface at the crater floor until an equilibrium is reached, where the surface charge is sufficiently strong to repel the electron cloud. At this point the electron fluid is balanced above by the plasma pressure. The electron pressure balance is determined by integrating equation (7) to obtain

$$\frac{1}{2}\epsilon_0 E^2\Big|_{z_f}^{z} = n(z)kT|_{z_f}^{z}\,, \tag{8}$$

where $E = -\mathrm{d}\phi/\mathrm{d}z$. The equation above leads to a family of solutions, parameterized by the integration constant

$$\Delta P_e(z = z_f) = \frac{1}{2}\epsilon_0 E^2(z_f) - n_{ef}kT. \tag{9}$$

A unique steady-state solution of the electron cloud and related potential is obtained by requiring a pointwise electron pressure balance throughout the entire extent of the column:

$$\Delta P_e(z) = 0, \quad \forall z. \tag{10}$$

This convenient choice is found to produce a reasonable first approximation of the surface potential at the crater floor, leaving for future work the additional surface charge buildup owing to suprathermal electrons. With the electron pressure balance condition above holding in particular at solar wind layer z_f, the integration constant $\Delta P_e(z_f)$ in equation (8) vanishes, and the equation reduces to

$$\frac{1}{2}\epsilon_0 E^2(z) = n_{ef}kT \exp(e\phi(z)/kT_e). \tag{11}$$

In addition, the electron pressure balance condition provides important boundary information. At the upper boundary, the solar wind layer, we obtain the effective ambipolar field

$$E_A = E(z_f) = -\left(\frac{2n_{ef}kT}{\epsilon_0}\right)^{1/2}, \tag{12}$$

which accelerates the expansion front downward toward the crater surface. As described later on, this ambipolar field along the upper boundary of the electron cloud implies a positive image charge layer in the (mostly) quasi-neutral plasma above. In this manner the model maintains overall charge neutrality.

At the lower boundary, the crater surface, the field solution is used to predict the steady-state surface charge

$$\sigma_S = 2\epsilon_0 E(z = S) = -2\left[2\epsilon_0 n_{ef}kT_e \exp(e\phi_S/kT_e)\right]^{1/2}, \tag{13}$$

written in terms of the solution to the surface potential ϕ_S, which is obtained below. Integrating equation (11), with $E = -\mathrm{d}\phi/\mathrm{d}z$, results in the following distribution for the electric potential:

$$\frac{e}{kT_e}(\phi - \phi_f) = -2\ln\left(1 + \frac{z_f - z}{\sqrt{2}\lambda_{D0}}\right). \tag{14}$$

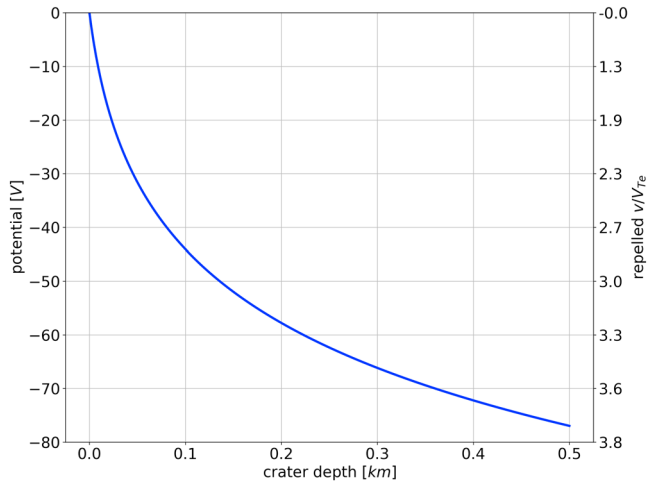

Figure 2. Surface potential (left axis) and equivalent repelled electron speed (right-hand axis) versus crater depth, at fixed $x = 0$, going down to $z = -0.5$ km.

It follows that, in this simple formulation, the steady-state potential distribution is independent of crater depth S. The resulting distribution of the electron cloud density is

$$n_e(z) = n_{ef}\left(1 + \frac{z_f - z}{\sqrt{2}\lambda_{D0}}\right)^{-2}. \tag{15}$$

We note that equation (11) and its solution are identical to the electron cloud analysis that Crow et al. (1975) obtained by enforcing a boundary condition at infinity; $\phi(\infty) = -\infty$, $\mathrm{d}\phi/\mathrm{d}z(\infty) = 0$. In our case, by maintaining a finite boundary, the present formulation produces additional information about the steady-state potential and surface charge at the crater floor. The steady-state surface charge, as a function of the crater depth S, is given by

$$\frac{\sigma_S}{en_{e0}\lambda_{D0}} = -2\sqrt{2}\frac{n_{ef}}{n_{e0}}\left(1 + \frac{z_f - S}{\sqrt{2}\lambda_{D0}}\right)^{-1}. \tag{16}$$

Here the upper boundary electron density, n_{ef}, will be given by the x dependent self-similar solution, producing the 2-D effect in this 1-D solution.

This completes the fluid description of a 1-D bounded electron clouded column, to be extended below into a 2-D crater. To illustrate this initial result, Figure 2 presents the surface potential at $x = 0$, varying the crater depth down to 500 m. Here the incoming solar wind plasma is characterized by $kT_e = 11$ eV and $n_{e0} = 5.0 \times 10^6$ m^{-3}. At 500 m, the surface potential generated by the electron cloud is found to be approximately −77 V. Equivalently, we show on the right-hand axis the corresponding maximum electron speed to be repelled by the surface potential. The speed is normalized by the electron thermal speed V_{Te}. The calculation shows that electrons entering a 500-m crater at a downward speed slower than $3.7v_e$ are repelled away back into the solar wind.

Comparing this result with simulations by Zimmerman et al. (2011), we find closer agreement with simulated values in the absence of a crater surface (repelled $v \sim 3V_{Te}$) than with a crater surface (repelled $v \sim 5V_{Te}$). This can be attributed to the absence of kinetic effects in our present fluid model. Incorporating kinetic effects would allow suprathermal electrons—moving much faster than typical thermal speeds—to penetrate the potential barrier and further contribute to the surface charge. The steady-state surface potential would then be converged asymptotically, in a negative feedback cycle, as fewer electrons penetrate the potential barrier. Additionally, Halekas et al. (2005) showed that empirical data from Lunar Prospector is better fit to a κ distribution electron model rather than a Maxwellian. Thus, a more accurate analysis of the surface potential, and associated negative feedback for plasma expansion, will require more accurate accounting of the hot electrons found in the upper end of the velocity distribution. This is left for future work.

3.1. Two-Dimensional Boundary Matching

In order to capture the 2-D wake structure within a crater, we follow the approach of Farrell et al. (2010), mapping an ensemble of 1-D solutions in (t, z) into 2-D solutions in (x, z) using $t = x/V_{\mathrm{sw}}$ (assuming a constant solar wind horizontal flow speed V_{sw}). In the present model, this approach is extended by matching the upper boundary parameters of the 1-D electron cloud solution with the expansion front of the self-similar solution, $\xi_f = -Mz_f/x$, parametrized by

$$\frac{z_f(x)}{\lambda_{D0}} = \left[1 - 2\ln\left[\frac{x}{\lambda_{D0}M}\right]\right]\frac{x}{\lambda_{D0}M}. \tag{17}$$

Combining the parameterization above with the general self-similar solution in equation (1), the boundary conditions along the expansion front become

$$v_f/C_i = \xi_f(x) + 1 = 2\ln\left(\frac{x}{\lambda_{D0}M}\right), \tag{18}$$

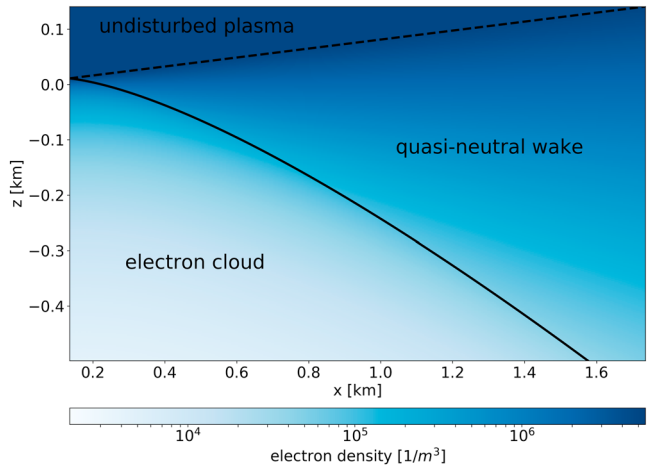

Figure 3. The electron density distribution above a 500 m lunar crater, using solar wind parameters $kT_e = 11$ eV and $n_{e0} = 5.0 \times 10^6$ m^{-3}. The rarefaction front (dashed line) and expansion front (solid line) outline the domain of the self-similar solution, which is extended here into the electron cloud cavity. This solution maintains a continuous electron density across the entire region.

$$n_{\mathrm{ef}}/n_{e0} = e^{-(\xi_f(x)+1)} = \left(\frac{x}{\lambda_{D0}M}\right)^{-2}, \tag{19}$$

$$\frac{e\phi_f}{kT_e} = -(\xi_f(x)+1) = -2\ln\left(\frac{x}{\lambda_{D0}M}\right). \tag{20}$$

These boundary conditions lead to a jump in the electric field, similar to that of the rarefaction front in the original formulation (Gurevich et al., 1966). Each electric field jump corresponds to a local charge layer, in this case an ion front on top of the continuous background of electrons. Approximating the thin charge layers as δ-functions, the model predicts the following respective charge densities at the rarefaction and expansion (quasi-neutral boundary) fronts:

$$\frac{\sigma_r}{en_{e0}\lambda_{D0}} = \frac{M}{x}, \tag{21}$$

$$\frac{\sigma_f}{en_{e0}\lambda_{D0}} = (\sqrt{2}-1)\frac{M}{x} \tag{22}$$

By adopting this simple matching of the self-similar neutral region with the Poisson solution of the electron cloud, we generate a closed analytic solution—approximately correct over long length and time scales—that predicts the surface charge and potential at the crater floor. Similarly, the surface charge layer described by equation (22) represents the positive image charge formed at the interface with the negative electron cloud. While neglecting to resolve the ion front boundary layer width observed in numerical models (Crow et al., 1975; Medvedev, 2011; Mora, 2003), the new model represents a substantial improvement in our understanding of the surface charge and near-surface environment downstream of an obstruction on the lunar surface. Furthermore, this analytic approach facilitates rapid computation as well as the flexibility to easily adapt the boundary conditions to incorporate additional physics in future studies.

4. Calculations of the Extended Wake Structure

The model described above extends the self-similar solution into the electron cloud cavity that forms beyond the quasi-neutral expansion front. As an illustrative case, we present the resulting plasma wake structure and resulting surface potential for a flat 500-m deep crater. The nominal electron density and temperature of the undisturbed plasma are taken to be 5×10^6 m^{-3} and 11 eV, respectively. The uniform horizontal solar wind flow speed is taken to be 400 km/s.

Figure 3 shows the electron density throughout the extended wake region. Note the continuous density distribution across the quasi-neutral expansion front (solid line) and across the rarefaction front (dashed

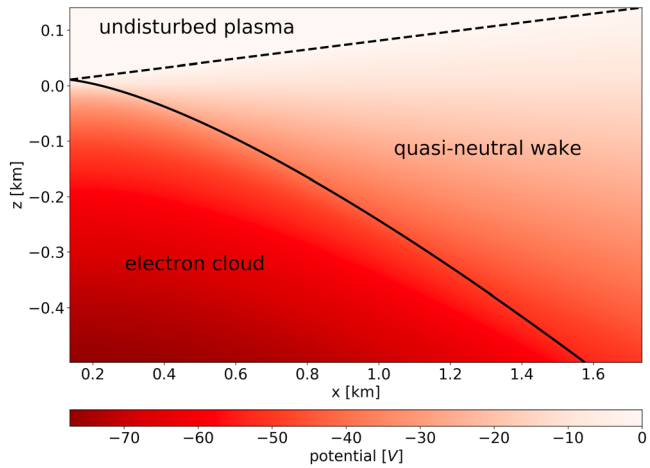

Figure 4. The electrostatic potential distribution associated with the parameters of Figure 3. The zero reference potential is defined by the rarefaction front. Like the electron density, the potential is continuous throughout the entire region.

line). While the rarefaction front is a linear process of thermal expansion, the expansion front is accelerated downward by the ambipolar electric field. This charge separation effect produces the logarithmic shape of the expansion front, manifest in equation (4), which differs from the linear self-similar expansion parameter in equation (3). In addition, the ambipolar field causes the electron density to decrease with distance from the quasi-neutral plasma. In this case, the density is found to decrease by 2 orders of magnitude, from $\sim 10^6$ to $\sim 10^4$ particles per cubic meter.

In Figure 4, we show the corresponding electrostatic potential distribution associated with Figure 3. The rarefaction front of the self-similar wake region defines the zero reference potential. An interesting feature of this extended model is the 2-D structure which emerges, despite the 1-D nature of the model. This effect, which is intrinsic in the self-similar solution, propagates into the electron cloud extension via the boundary condition along the expansion front. Hence, the more moderate (less negative) surface potential downstream, ~ -40 V near where the ion wake strikes the surface. Near the left-hand edge of the crater floor, at the base of the crater wall, the calculated surface potential is ~ -80 V (as also portrayed in Figure 2). This result demonstrates our closed, consistent solution of the surface potential in the electron cloud region, which is the major objective of this work.

The electric field associated with the potential distribution discussed above is shown in Figure 5. Again, substantially different behavior is observed in the three regions. Starting along the top, the undisturbed plasma maintains zero field. Next, the solution in the quasi-neutral wake region is constant along a given vertical slice, since the self-similar electric field scales as $1/t \sim 1/x$, uniform in z. Finally, the electron cloud region exhibits a peak field just below the expansion front, followed by a decline proportional along a vertical slice to $1/z$.

Two different vertical (z) slices, each at a different fixed x value, are shown in Figure 6 in arbitrary units. This is equivalent to a pair of time slices for the expanding wake. The potential, field, and charge density are, respectively, represented by continuous, dashed, and dotted lines. Looking at the electric field (dashed) line, we observe the backward propagating rarefaction front and forward propagating expansion front.

We note the positive charge layers, given, respectively, by equations (21) and (22) for the rarefaction and expansion fronts. The present δ-function charge layers are analogous to the finite peaks observed in simulations by Mora, (2003, their Figure 1). Furthermore, the corresponding electric field jumps in our Figure 6, coinciding with the positive charge layers, are analogous to the sharp electric field transitions in Mora's Figure 2. Unlike the simple self-similar model, which does not predict the system behavior beyond the expansion front, the present model clearly shows diminishing charge density and electric field in the rightmost section of the curves in Figure 6. This qualitative structure, including both the positive and negative charge regions, is a necessary requirement for the overall charge balance.

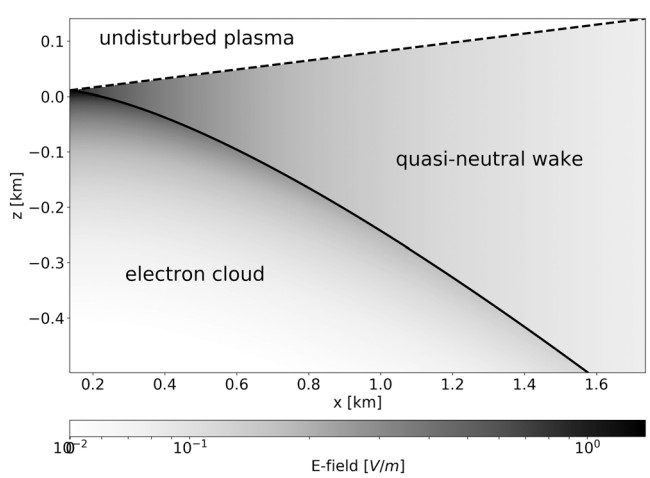

Figure 5. The electric field distribution associated with the parameters of Figure 3. The field discontinuity results from the self-similar approximation, which neglects the sub-Debye length characteristics at the rarefaction and expansion fronts.

Various numerical models show that in reality these electric field jumps correspond to steep but continuous distributions (Crow et al., 1975; Medvedev, 2011; Mora, 2003). Given our present interest in the surface potential of the crater floor, it is beyond the scope of this paper to resolve the ion front boundary layer structure. We justify this decision by referring to the detailed boundary layer analysis of Medvedev (2011), where substantial discrepancies in the bulk plasma behavior are found for $\omega_i t > 350$. Here the characteristic timescale ω_i is the ion plasma frequency, defined in section 2. In contrast, the present study has a typical timescale of $\omega_i t \approx 15$ for the expansion front to reach the surface.

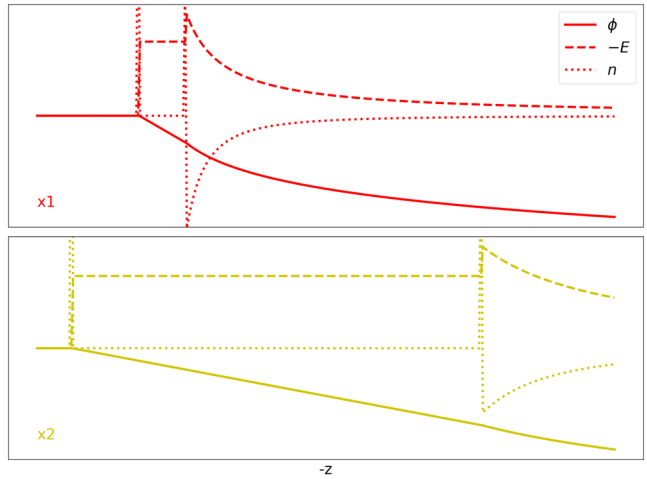

Figure 6. Two vertical slices associated with the parameters of Figure 3, including the potential (solid), field (dashed), and charge density (dotted), in arbitrary units. This view demonstrates the forward propagation of the expansion front and the backward propagation of the rarefaction front, with field and charge density discontinuities owing to the self-similar quasi-neutral approximation.

Figure 7 shows the average space charge density in unit charge per cubic meter. This figure is somewhat equivalent to the left-hand side of Figure 3 but emphasizes a prominent feature of this extended model, namely, large-scale space charge. Since both the undisturbed plasma and the central wake region are quasi-neutral, the appearance of large-scale space charge is unique to the electron cloud. Whereas a typical plasma can develop a thin nonneutral sheath at a surface interface, on the order of the Debye length for charge separation (∼10 m for the given parameters), the electron cloud spans many Debye lengths. As discussed in section 1, this novel physics environment poses a unique grounding challenge for explorers traversing the lunar terrain.

Lastly, Figure 8 shows the average downward speed of the plasma particles. The average speed of the Maxwellian electron cloud is zero, so the remaining result is attributed solely to the ions. We plot only the vertical component of the velocity, to separate out the uniform horizontal solar wind flow velocity. This view highlights the ion flow behavior under the influence of the ambipolar field. The calculation shows that by the time the ions reach the crater surface, they develop a velocity of ~ -150 km/s, comparable to the horizontal flow speed (400 km/s). This result may be consequential for its effect on surface sputtering.

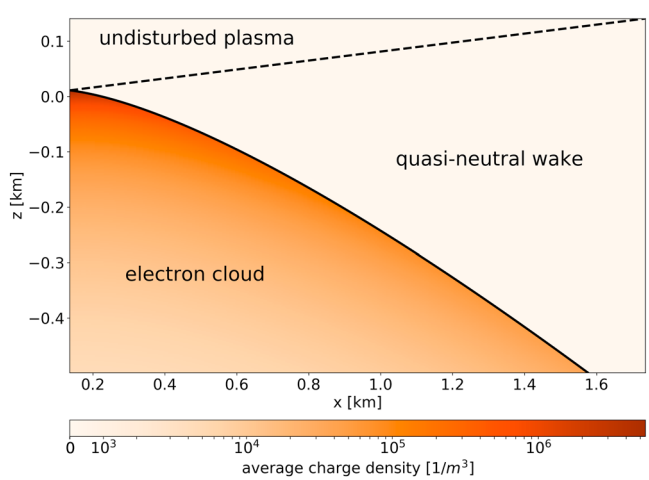

Figure 7. The average charge density associated with the parameters of Figure 3. This view emphasizes the unique feature of the negatively charged electron cloud region, compared to the expanding quasi-neutral plasma.

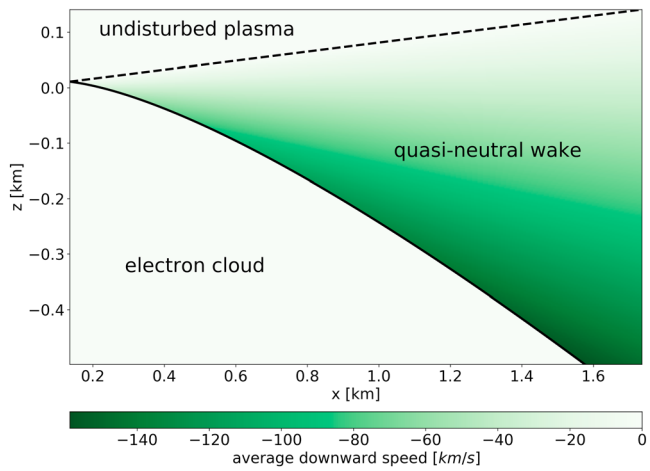

Figure 8. The average downward velocity associated with the parameters of Figure 3. Net velocity in steady state is found only in the quasi-neutral region, described by the self-similar solution.

5. Summary

We have developed an analytical model of the plasma wake structure as the solar wind flows over an obstruction on an airless body. This is achieved by deriving a closed form solution of the electron cloud and its associated surface potential, in the cavity formed below the bulk quasi-neutral plasma flow. We then merge the solution of the electron cloud region with the expansion front of the well-known self-similar solution, which describes the quasi-neutral region. In doing so, we obtain the downstream solution to the surface potential both under the electron cloud and into the regions were the ions intercept the surface. By extending the theoretical framework for this plasma wake phenomenon, we provide a better understanding of observations in recent particle-in-cell simulations (Zimmerman et al., 2011).

From a theoretical standpoint, this study establishes an understanding of a novel plasma environment, where a negative space charge is naturally confined on length scales much greater than the Debye length of the undisturbed plasma. In addition, the general phenomenon of the solar wind wake structure may impact the surface chemistry of airless bodies.

From a practical perspective of roving astronauts, the model provides an estimate of the electrical grounding conditions on the crater surface. The electron cloud zone along the surface, spanning several times the crater depth, provides little dissipation to oppose the buildup of triboelectric charge. This work provides a basis for more detailed studies on tribocharging and dissipation of roving explorers in a low-dissipation plasma environment.

Our analytic formulation provides flexibility in adding additional physics in the future. Possible extensions include kinetic effects, solar wind inflow angles, magnetic fields, secondary electrons, and dust lofting. Synthetic validation could be established by a laboratory experiment with appropriately scaled plasma flow and density. In situ validation could be obtained by a lander carrying a plasma instrument.

Acknowledgments
Research by Dov Rhodes was supported by an appointment to the NASA Postdoctoral Program at the NASA Goddard Space Flight Center, administered by the Universities Space Research Association under contract with NASA. Research by William Farrell was supported by NASA SSERVI Award DREAM2. No experimental data was produced in this research.

References

Carrier, W. D., Olhoeft, G. R., & Mendell, W. (1991). Physical properties of the lunar surface. In *Lunar Sourcebook* (pp. 475–594). Cambridge: Cambridge University Press.

Crow, J. E., Auer, P. L., & Allen, J. E. (1975). The expansion of a plasma into a vacuum. *Journal of Plasma Physics*, *14*(01), 65. https://doi.org/10.1017/S0022377800025538

Ergun, R. E., Malaspina, D. M., Bale, S. D., McFadden, J. P., Larson, D. E., Mozer, F. S., et al. (2010). Spacecraft charging and ion wake formation in the near-Sun environment. *Physics of Plasmas*, *17*(7), 72903. https://doi.org/10.1063/1.3457484

Farrell, W., Halekas, J., Fatemi, S., Poppe, A., Hartzell, C., Marshall, J., et al. (2017). Anticipated electrical environment at Phobos: Nominal and solar storm conditions. *Advances in Space Research*, *62*, 2199–2212. https://doi.org/10.1016/j.asr.2017.08.009

Farrell, W. M., Stubbs, T. J., Delory, G. T., Vondrak, R. R., Collier, M. R., Halekas, J. S., & Lin, R. P. (2008b). Concerning the dissipation of electrically charged objects in the shadowed lunar polar regions. *Geophysical Research Letters*, *35*, L19104. https://doi.org/10.1029/2008GL034785

Farrell, W. M., Stubbs, T. J., Halekas, J. S., Delory, G. T., Collier, M. R., Vondrak, R. R., & Lin, R. P. (2008a). Loss of solar wind plasma neutrality and affect on surface potentials near the lunar terminator and shadowed polar regions. *Geophysical Research Letters*, *35*, L05105. https://doi.org/10.1029/2007GL032653

Farrell, W. M., Stubbs, T. J., Halekas, J. S., Killen, R. M., Delory, G. T., Collier, M. R., & Vondrak, R. R. (2010). Anticipated electrical environment within permanently shadowed lunar craters. *Journal of Geophysical Research*, *115*, E03004. https://doi.org/10.1029/2009JE003464

Farrell, W. M., Stubbs, T. J., Vondrak, R. R., Delory, G. T., & Halekas, J. S. (2007). Complex electric fields near the lunar terminator: The near-surface wake and accelerated dust. *Geophysical Research Letters*, *34*, L14201. https://doi.org/10.1029/2007GL029312

Gurevich, A. V., Pariiskaya, L. V., & Pitaevskii, L. P. (1966). Self-similar motion of rarefied plasma. *Soviet Physics JETP*, *22*, 449.

Gurevich, A. V., & Pitaevsky, L. P. (1975). Non-linear dynamics of a rarefied ionized gas. *Progress in Aerospace Sciences*, *16*, 2270–272. https://doi.org/10.1016/0376-0421(75)90016-0

Halekas, J. S., Bale, S. D., Mitchell, D. L., & Lin, R. P. (2005). Electrons and magnetic fields in the lunar plasma wake. *Journal of Geophysical Research*, *110*, A07222. https://doi.org/10.1029/2004JA010991

Halekas, J. S., Mitchell, D. L., Lin, R. P., Hood, L. L., Acuña, M. H., & Binder, A. B. (2002). Evidence for negative charging of the lunar surface in shadow. *Geophysical Research Letters*, *29*(10), 1435. https://doi.org/10.1029/2001GL014428

Jackson, T. L., Farrell, W. M., Killen, R. M., Delory, G. T., Halekas, J. S., & Stubbs, T. J. (2011). Discharging of roving objects in the lunar polar regions. *Journal of Spacecraft and Rockets*, *48*(4), 700–704. https://doi.org/10.2514/1.51897

Jackson, T. L., Farrell, W. M., & Zimmerman, M. I. (2015). Rover wheel charging on the lunar surface. *Advances in Space Research*, *55*(6), 1710–1720. https://doi.org/10.1016/j.asr.2014.12.027

Killen, R. M., Hurley, D. M., & Farrell, W. M. (2012). The effect on the lunar exosphere of a coronal mass ejection passage. *Journal of Geophysical Research*, *117*, E00K02. https://doi.org/10.1029/2011JE004011

Medvedev, Y. V. (2011). Ion front in an expanding collisionless plasma. *Plasma Physics and Controlled Fusion*, *53*(12), 125007. https://doi.org/10.1088/0741-3335/53/12/125007

Mora, P. (2003). Plasma expansion into a vacuum. *Physical Review Letters*, *90*(18), 185002. https://doi.org/10.1103/PhysRevLett.90.185002

Mora, P., & Pellat, R. (1979). Self-similar expansion of a plasma into a vacuum. *Physics of Fluids*, *22*(12), 2300. https://doi.org/10.1063/1.862541

Ogilvie, K. W., Steinberg, J. T., Fitzenreiter, R. J., Owen, C. J., Lazarus, A. J., Farrell, W. M., & Torbert, R. B. (1996). Observations of the lunar plasma wake from the WIND spacecraft on December 27, 1994. *Geophysical Research Letters*, *23*(10), 1255–1258. https://doi.org/10.1029/96GL01069

Poppe, A. R., Piquette, M., Likhanskii, A., & Horányi, M. (2012). The effect of surface topography on the lunar photoelectron sheath and electrostatic dust transport. *Icarus*, *221*(1), 135–146. https://doi.org/10.1016/j.icarus.2012.07.018

Poppe, A., Zimmerman, M., Halekas, J., & Farrell, W. (2015). The electrostatic plasma environment of a small airless body under non-aligned plasma flow and UV conditions. *Planetary and Space Science*, *119*, 111–120. https://doi.org/10.1016/j.pss.2015.06.001

Samir, U., Wright, K. H., & Stone, N. H. (1983). The expansion of a plasma into a vacuum: Basic phenomena and processes and applications to space plasma physics. *Reviews of Geophysics*, *21*(7), 1631. https://doi.org/10.1029/RG021i007p01631

Scheiner, B., Baalrud, S. D., Yee, B. T., Hopkins, M. M., & Barnat, E. V. (2015). Theory of the electron sheath and presheath. *Physics of Plasmas*, *22*(12), 123520. https://doi.org/10.1063/1.4939024

Stubbs, T. J., Vondrak, R. R., & Farrell, W. M. (2006). A dynamic fountain model for lunar dust. *Advances in Space Research*, *37*(1), 59–66. https://doi.org/10.1016/j.asr.2005.04.048

Tribble, A., Pickett, J., D'Angelo, N., & Murphy, G. (1989). Plasma density, temperature and turbulence in the wake of the shuttle orbiter. *Planetary and Space Science*, *37*(8), 1001–1010. https://doi.org/10.1016/0032-0633(89)90054-8

Zimmerman, M., Farrell, W., & Poppe, A. (2014). Grid-free 2D plasma simulations of the complex interaction between the solar wind and small, near-Earth asteroids. *Icarus*, *238*, 77–85. https://doi.org/10.1016/j.icarus.2014.02.029

Zimmerman, M. I., Farrell, W. M., Stubbs, T. J., Halekas, J. S., & Jackson, T. L. (2011). Solar wind access to lunar polar craters: Feedback between surface charging and plasma expansion. *Geophysical Research Letters*, *38*, L19202. https://doi.org/10.1029/2011GL048880

Zimmerman, M. I., Jackson, T. L., Farrell, W. M., Stubbs, T. J, & E00K03 (2012). Plasma wake simulations and object charging in a shadowed lunar crater during a solar storm. *Journal of Geophysical Research*, *117*, E00K03. https://doi.org/10.1029/2012JE004094